Preparation, Characterization and Application of a Home–made Graphene for the Removal of Congo Red From Aqueous Solutions

Temilolu J. Popoola
Federal University of Technology Akure
Afamefuna E. Okoronkwo
Federal University of Technology Akure
Olugbenga O. Oluwasina
Federal University of Technology Akure
Matthew A. Adebayo (adebayomao@gmail.com)
Federal University of Technology https://orcid.org/0000-0002-6009-4075

Research Article

Keywords: Coal, Graphene, Ethylene diaminetetraacetic acid, Congo red, Liu model, Avrami model

Posted Date: February 8th, 2021

DOI: https://doi.org/10.21203/rs.3.rs-166094/v1

Preparation, characterization and application of a home–made graphene for the removal of Congo red from aqueous solutions

Temilolu J. Popoola, Afamefuna E. Okoronkwo, Olugbenga O. Oluwasina and Matthew A. Adebayo*

Department of Chemistry, The Federal University of Technology, Akure, Ondo State, Nigeria

*All correspondence to: adebayoma@futa.edu.ng; +234 703 567 1346 (M.A. Adebayo)

Abstract

Ethylene diaminetetraacetic acid (EDTA) functionalized graphene was synthesized from Nigerian coal using a chemical exfoliation method and the graphene was applied for the removal of Congo red dye from aqueous solutions. The synthesized coal graphene and the raw coal were characterized using Fourier transform infrared (FTIR) spectroscopy, X-ray diffraction (XRD) spectroscopy, Scanning electron microscopy and Energy (SEM)–Energy dispersive X-ray (EDX) spectroscopy. The SEM data revealed surface roughness which is enhanced in the prepared graphene while the EDX revealed an increase in carbon, the main constituent of graphene, from about 26% in the raw coal to about 80% in the prepared graphene. Various adsorption parameters, such as pH, contact time, concentration of Congo red and temperature, were varied for the removal of the dye using raw coal and the synthesized coal graphene. The Liu isotherm gave the best fit of the equilibrium data than the Langmuir, Freundlich and Dubinin-Radushkevich models. The maximum adsorption capacities of the raw coal and synthesized coal graphene at 25 °C are 109.1 mg/g and 129.0 mg/g, respectively. The Avrami fractional order kinetic model was the best model for description of the kinetic data. The model had the lowest values of standard deviation than the pseudo-first order and pseudo-second order models. The adsorption process of the two materials occurred *via* two stages as proved by intraparticle diffusion model. The adsorption process of the Congo red removal was spontaneous, feasible and endothermic. The study conclusively revealed the graphene nanomaterial to be a viable adsorbent for textile wastewater treatment.

Keywords: Coal; Graphene; Ethylene diaminetetraacetic acid, Congo red; Liu model; Avrami model

Introduction

Over time, industrialization and population explosion have led to an upward surge in the utilization of dyes for printing and coloring by industries, particularly the textile industry (Hairom et al. 2014) and a lot of wastewater, from plastic, paper, printing, textile and dyeing industries, is generated during printing, production and dyeing processes (Chong et al. 2014; Adebayo et al. 2014; Adebayo 2019). Dyes, which are non-biodegradable, constitute a major source of water pollution and the menace is becoming a major environmental issue worldwide. The presence of molecules of dyes in

water is associated with the generation of an aesthetic problem, water coloration, increment in chemical oxygen demand, reduction in sunlight penetration for aquatic plants and can lead to allergies, mutation and cancer (Rovani et al. 2014; dos Santos et al. 2014).

Congo red (CR) is the disodium salt of the most widely used direct dye in the textile industry due to its chromaticity (Yao et al. 2016). Various types of dye, particularly the Congo red, are critical sources of wastewater contamination due to its increased oxygen demand and high biological toxicity after indiscriminate dumping in water bodies (Robinson et al. 2001). The presence of Congo red in water bodies results in unpleasant changes in the color of water and its presence even in trace amounts can adversely affect living things due to inhibitory effects on photosynthesis (Tabrez et. al. 2004). The anaerobic breakdown and incomplete bacterial degradation of dyes often result in the production of toxic amines, which pose serious threat to mankind (Weber and Wolfe 1987). For example, Congo red, a synthetic dye is largely non-biodegradable and carcinogenic. Therefore, its presence in the ecosystem even in trace amounts is of great environmental concern due to adverse effect on human health and the economy. These issues, therefore require prompt and effective remediation of textile wastewater to reduce the levels of pollution of Congo red to permissible limits (Zhang et al. 2014).

To this end, various methods have been adopted for the effective removal of toxic dyes from solutions, such techniques include but not limited to adsorption, chemical precipitation, ion exchange, reverse osmosis and membrane filtration (Thue et al. 2016; Ribas et al. 2020). Physical adsorption has been reported to be a proficient method for this process because of its simplicity, cost effectiveness, and efficiency (Kumari et al. 2016; Adebayo et al. 2020).

Over the past decade, carbonaceous materials have been of great interest to researchers because of their uniqueness, composition and diversity. A case in point is activated carbon, which has been investigated and shows promising result in the effective treatment of wastewater owing largely to its large surface area and mechanical stability (Suhas et al. 2017). However, due to the high energy consumption and greenhouse gas emission of coal during preparation of activated carbon (Alhashimi and Aktars 2017), its application has been limited. It is therefore pertinent to source for suitable alternative routes with less risk. Coal and other derivatives are common adsorbents for the treatment of textile wastewater and as a solid source raw material with high carbon content, it is stable at room temperature and quite easy to transport. Owing largely to environmental concerns of global warming, the primary function of coal as fuel for transport has been jettisoned (Shinn 1996). Presently, alternative uses of coal are being researched daily to cater for its large reserves while also making sure that its use is eco-friendly. The use of coal to synthesize graphene could open a new opportunity for coal as a non-conventional carbon source and provide reliability for large synthesis of graphene.

Nanomaterials, such as graphene, have been a point of focus for researchers because of their outstanding properties and diversity. The presence of various functional groups, binding sites, and large surfaces on these materials are the main characteristics that make graphene and graphene derivatives excellent adsorbents for the removal of countless pollutants, including toxic dyes, from aqueous effluents (Galashey and Polukhin 2014). The large specific surface area of graphene makes bonding sites available for modification by other compounds such as ethylenediaminetetraacetic acid (EDTA) (Cui et al. 2015). Ethylenediaminetetraacetic acid is an excellent precursor that serves many functions in the industrial sphere such as an auxiliary chemical in dyeing, as a stabilizer, a softener or even a metal complex in coordination titration (Repo et al. 2013). Ethylenediaminetetraacetic acid is a favourable option for modifying

adsorbent materials for the adsorption of dyes and can serve as a precursor for synthesis of a wide range of adsorbent composites with other materials such as graphene to enhance the adsorption capacity (Ali, 2012). A lot of nanomaterials, functionalized with EDTA, have been reported (Pang and Wilson 1991; Pang and Wilson 1993) and showed substantial efficiency adsorption towards dyes and heavy metals in aqueous solution but not much effort has been geared towards using EDTA as a precursor for graphene synthesis. Rehman et al. (2019) reported the synthesis of nanocrystalline Hematite using EDTA as a precursor which considers the feasibility of EDTA as a precursor rather than a modifier.

The current study, therefore, provided a pathway to prepare graphene from coal through a rapid and non-combustible method using EDTA as a precursor and chelating agent for the growth process and then investigate its effectiveness in the removal of Congo red from solution.

Materials and method

Sample preparation and characterization

Lignite was obtained from Kabba, Kogi State, Nigeria. The lump of coal was pulverized and sieved using a 625-µm mesh to obtain a sample of uniform particle size. All chemicals and reagents were procured from British Drug Houses (BDH) chemicals and were used as purchased.

Coal powder (5 g) was refluxed with EDTA (45 mL, 13.3 wt%) for 24 h, filtered and dried in a vacuum oven for 5 h at 120 °C. The obtained sample (2 g) was treated with aqueous hydrogen fluoride (25 mL, 40 wt%) for 2 h, ultrasonicated for 30 min and left for gravity separation. The sample was then washed with deionized water to neutral pH, centrifuged at 10,000 rpm and the solid sample was dried in the vacuum oven at 105 °C for 7 h to obtain a dry powder of graphene. The graphene obtained was named Synthesized Coal Graphene (SCG). The Raw Coal and the SCG were stored in a desiccator prior characterization and usage for adsorption experiments.

Fourier transform infrared (FTIR) spectroscopy, X-ray diffraction (XRD), scanning electron microscopy (SEM) and Energy-dispersive X-Ray (EDX) spectroscopy techniques were used to characterize the Raw Coal and SCG. The FTIR spectra were recorded in the spectral range of 4000 – 400 cm^{-1} using a FTIR spectrometer (Agilent Technologies, Germany). The XRD patterns were obtained using X-ray diffractometer (D8 advance, Bruker) with Cu Ka radiation (1.5406 Å) and at a scanning range of 0.5 – 130 (2 h). The SEM-EDX (VEGA TESCAN, Japan) was used to examine the surface morphology as well as to obtain the elemental composition of the synthesized material.

Adsorption experiment

To examine the adsorption behavior of the Congo red dye onto the synthesized graphene and raw coal, batch adsorption experiments were carried out. The experiments were performed using 25 mL sample tubes containing a 50 mg of adsorbent material and 20 mL of 25 mg/L – 800 mg/L Congo red in each flask. The effect of pH was investigated between pH 2 and 10; a 0.1 mol/L of HCl or NaOH was used to adjust the pH of the adsorbate solution. The sample tubes that contained adsorbent material and Congo red solution were then placed inside a thermostatic shaker and

agitated at 150 rpm for 0 – 360 min at varying temperature (25 °C – 65 °C). The dye solution-adsorbent systems were centrifuged and the aliquot of the supernatant was analyzed on a UV-Visible spectrophotometer (Shimadzu, Japan) at 497 nm to obtain the absorbance readings of unadsorbed dye after adsorption process. The concentration of the dye left in the solution after the experiment was subsequently calculated. The quantity of dye adsorbed at equilibrium, Q_e (mg/g), was evaluated using **Equation 1**.

$$Q_e = \frac{(C_o - C_e)}{w} \cdot V \qquad (1)$$

where C_o is the initial Congo red concentration in mg/L, C_e is the final (equilibrium) Congo red concentration in mg/L, V is the volume of the dye solution in L, and w is the weight of the adsorbent used in for the batch adsorption experiment in g.

Results and discussion

Characterization of Raw Coal and Synthesized Coal Graphene (SCG)

Graphene was prepared from a local coal using EDTA as a surface modifier. To know the features of the Raw Coal and SCG, the two materials were characterized using SEM-EDX, XRD and FTIR.

Figures 1a and **b** show the SEM images of the Raw Coal and SCG, respectively. The SEM images show irregular solid block materials with seemingly rough surfaces, which can promote adherence of the adsorbate. The raw coal image shows some impurities (highlighted in red) attached to the surface of the solid but impurities are absent in the SCG (Sohn et al. 2014). Similarly, the Raw Coal displayed a relatively large particles, which were broken down in SCG as a result of physical and chemical treatments. The HF is a strong acid that removed all extraneous materials present on the solid surface of the coal leaving the solid mass of SCG behind (Yang et al. 2007).

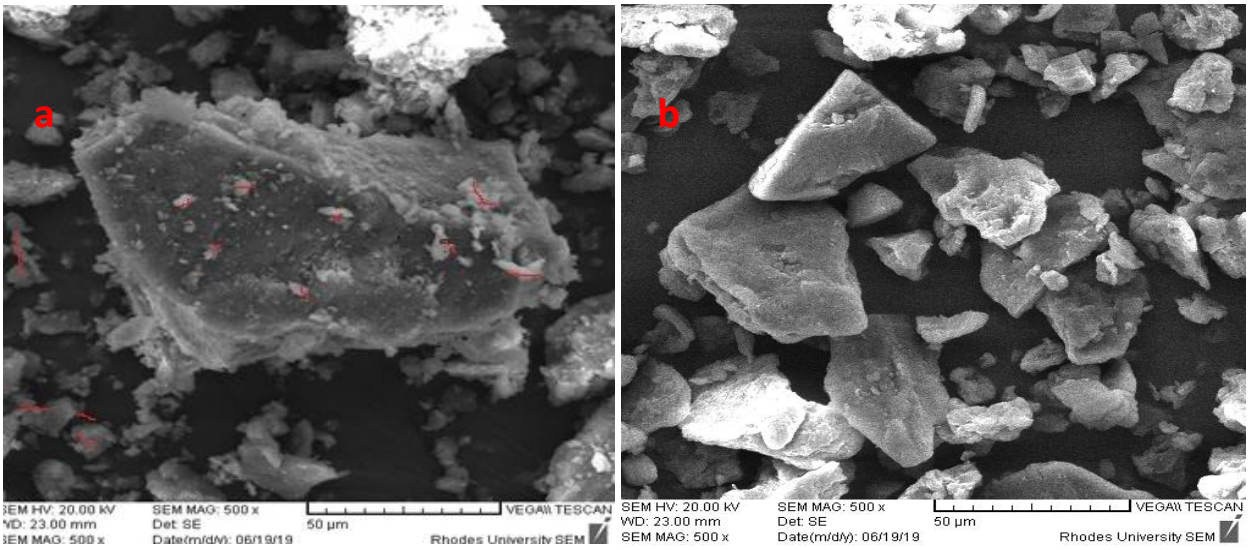

Figure 1. Scanning electron micrographs at 500x magnification of (**a**) Raw Coal and (**b**) SCG

The Energy-dispersive X-ray data of the Raw Coal and SCG are presented in **Table 1**. The EDX micrographs of the samples are shown in **Figure 2**. The elemental composition of the coal is: 20% carbon, 11% aluminum, 12% silicon, oxygen 55% and others at less than 2%. The EDX micrograph of SCG (**Figure 2a**) revealed a significant weight increase in carbon content compared to the spectrum of Raw Coal (**Figure 2a**). A 64% increase was observed and this increase is largely due to the various treatment processes carried out on the raw coal sample to obtain SCG. The strong carbon peak observed is also in agreement with high carbon percentage expected in graphene (Ghann et al. 2019). It is evident that the various chemical and physical treatments, especially using EDTA, in preparing SCG had a profound effect in removing most of the metals and extraneous materials present. Ethylene diaminetetraacetic acid being a chelating agent will form complexes with the majority of the metals such as aluminum and titanium. The formed complex was eliminated from the synthesized material by acid treatment which was applied to the complex solution, leaving behind the material of interest (Rao et al. 2017).

Table 1. Elemental analysis (EDX) of Raw Coal and SCG

Raw Coal			SCG		
Element	**Weight (%)**	**Atomic (%)**	**Element**	**Weight (%)**	**Atomic (%)**
C	19.94	27.78	**C**	76.88	82.16
O	54.89	57.40	**O**	21.31	17.09
Al	10.78	6.680	**Si**	0.4200	0.1900
Si	12.16	7.250	**S**	1.400	0.5600
S	0.9100	0.4800			
Ti	0.4400	0.1500			
Fe	0.8800	0.2600			
Total	**100.0**		**Total**	**100.0**	

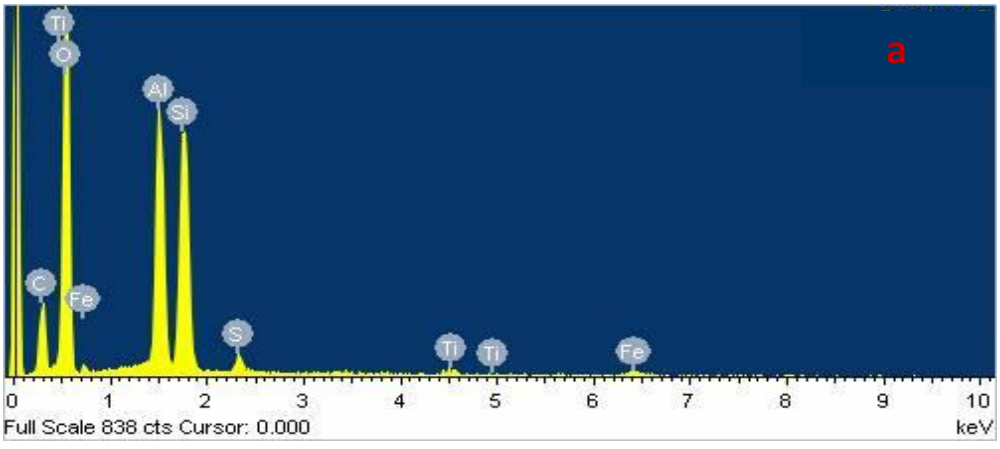

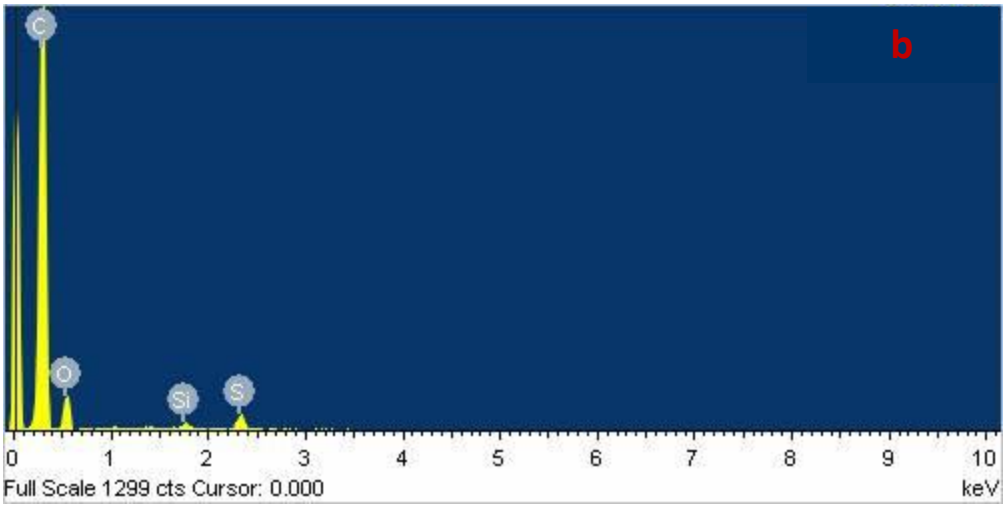

Figure 2. Energy-dispersive X-ray spectra of (**a**) Raw Coal and (**b**) SCG

The XRD spectra presented in **Figure 3** revealed that the diffractogram of the raw coal has $2\theta°$ values stretching between 11° to 65°. The raw coal displayed peaks of high intensity compared to the SCG, which is an indication of its higher crystallinity than the graphene precursor (Vassilev 1994). The chemical constituents of the raw coal are related to those reported by Querol et al. (2005). Siliceous minerals such as quartz (SiO_2) at $2\theta° = 26.245°$; kaolinite $Al_2(SiO_2O_5)(OH)_4$ at $2\theta° = 12.33°$, 20.238°, 21.57°, and 24.780°; chamosite ($Fe_3Si_2O_5(OH)_4$) at $2\theta° = 34.890°$; silicon carbide (SiC) at $2\theta° = 35.330°$; and katoite ($Ca_3Al_2(SiO)_4(OH)_8$) at $2\theta° = 38.846°$ are a few of such constituents all of which enhance crystallinity. In sharp contrast to the raw coal, SCG diffraction pattern shows a feature of amorphous carbon (a wide band between 10° and 35°) and a low level of crystalline phase (Thue et al. 2016). The low crystallinity level observed in SCG is a characteristic feature of the trace level of silicious materials from quartz (Ward et al. 1999; Thue et al. 2016). The peak width broadening contains micro-structural information that indicates uniform particle sizes of an amorphous nature. Summarily, the crystalline nature of the raw coal decreased substantially after treatment because sharp peaks were no longer observed in the synthesized coal graphene.

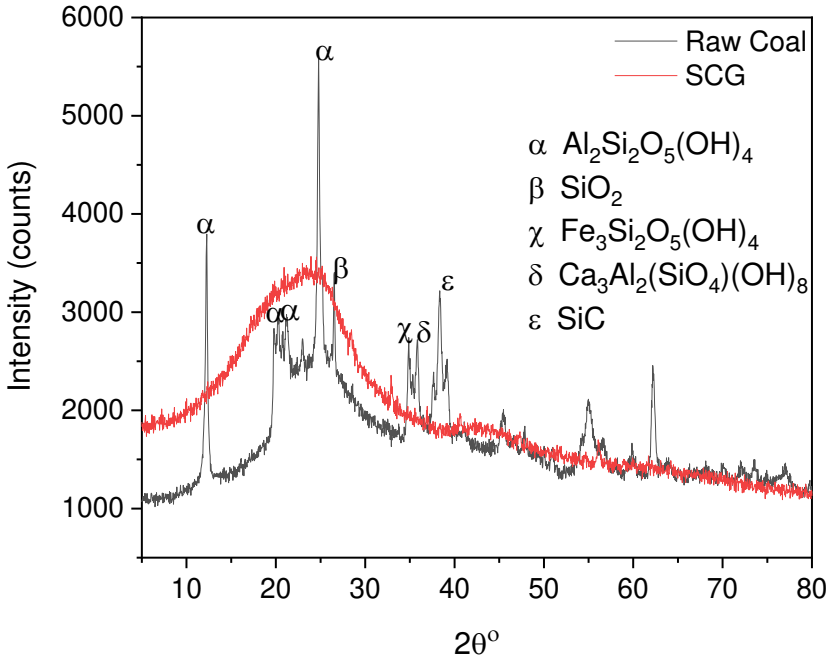

159

160 **Figure 3.** X-ray diffraction patterns of Raw Coal and SCG

161

162 The FTIR results presented in **Figures 4a** and **b** show the spectra of the SCG before and after adsorption of Congo
163 red, respectively. Graphene is a carbon material with no functional group (Suraj et al. 1997). In the functional group
164 region of the spectrum (**Figure 4a**), the bands in the range of 2083 cm^{-1} and 3690 cm^{-1} are overtone and combination
165 bands, which are not useful diagnostically while other vibrational frequencies might be due to carbon–carbon bonds
166 in the SCG. Consequently, **Figure 4a** confirmed the absence of functional groups in the SCG before application as an
167 adsorbent. The adsorbate contains functional groups such as benzene ring as well as amino, azo, and sulfonate groups.
168 **Figure 4b** showed a characteristic absorption band of amino group at 3205 cm^{-1} while the band at 1595 cm^{-1} is
169 ascribed to azo group. The stretching vibration at 1438 cm^{-1} is due to sulfate group and also an aromatic ring is seen
170 at 745 cm^{-1}. **Figure 4b** showed the activity of SCG as an adsorbent of Congo red. Hence, Congo red was adsorbed
171 onto the SCG (Suraj et al. 1997).

172

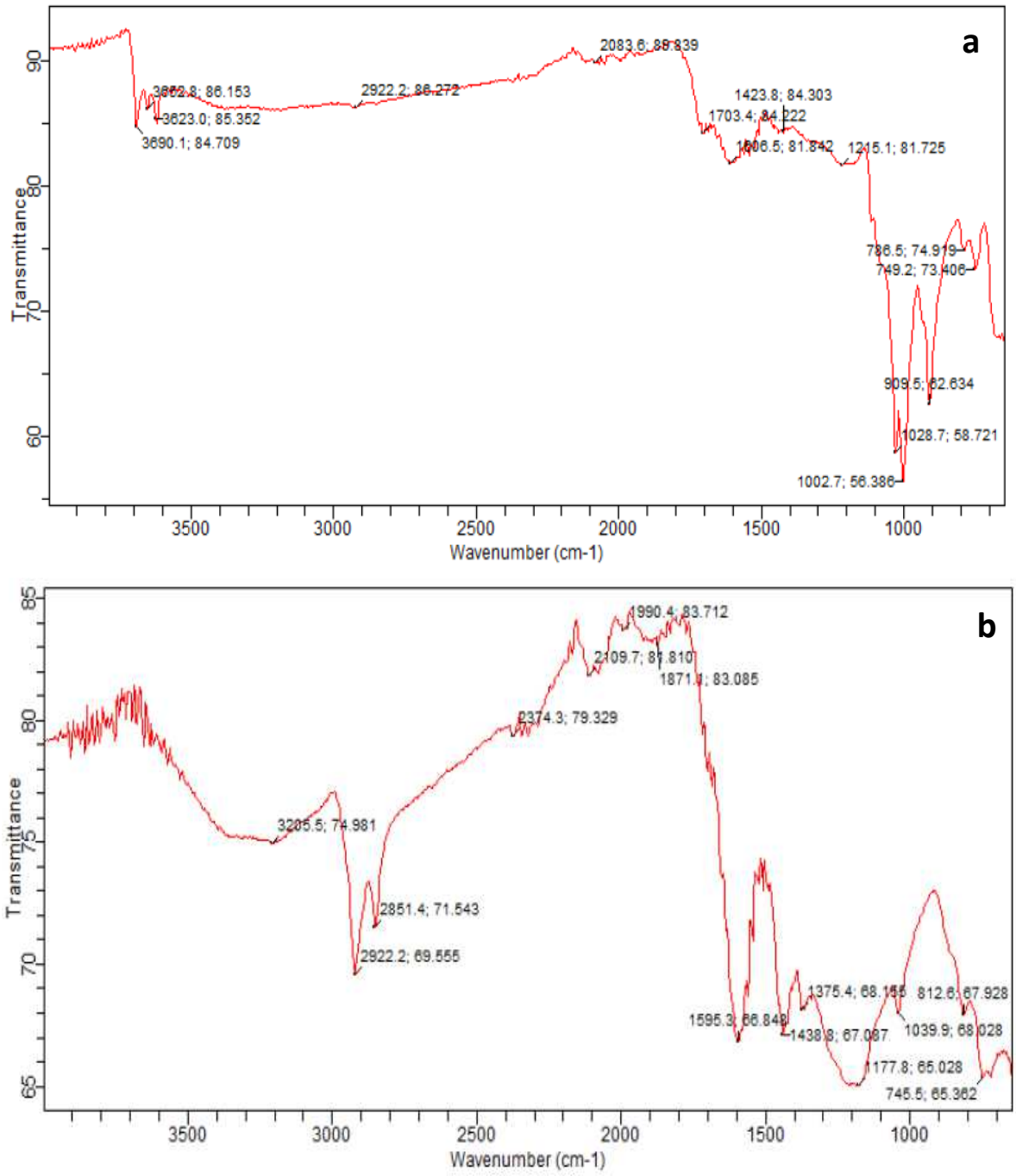

Figure 4. Fourier transform infrared spectra of (**a**) SCG before adsorption of Congo red and (**b**) SCG after adsorption of Congo red

Adsorption studies

pH Studies

The results of the effect of pH on the adsorption of Congo red using Raw Coal and SCG are presented in **Figure 5**. The adsorption of Congo red onto SCG was relatively steady across selected pH range with a maximum adsorption of 39.55 mg/g observed at pH 3 while adsorption capacity of Raw Coal for removal of Congo red decreased as we moved from acidic to alkaline region with maximum removal (24.77 mg/g) at pH 3. Congo red is dipolar and therefore it is an anionic and cationic in alkaline medium and acidic medium, respectively. However, as the pH of the Congo red dye decreases, the color of the solution changes from orange to dark blue (Stephen, 2000). This phenomenal color change, which solely depends on the pH of the dye solution, is a pointer to the ionic character of the Congo red molecule. This is because of the lone pair transition that happens upon acidification leading to a change in the wavelength of the red dye (Stephen, 2000). From **Figure 5**, the quantity of Congo red removed varied only slightly, especially for SCG. This behavior can be attributed to the unique properties of graphene such as mechanical and electrical stability (Shin, 2016). Nupearachchi (2017) reported effective adsorption capacities for nanoparticles synthesized from coal after extraneous materials have been removed from the raw materials. He concluded that the efficiency of adsorption increased because pore sites were opened up *via* the ultra-sonication process, which is similar to what is observed in this report. On the basis of the pH data, the optimum pH of the adsorption of Congo red onto the two adsorptive materials was 3, therefore pH 3 was chosen to conduct other experiments.

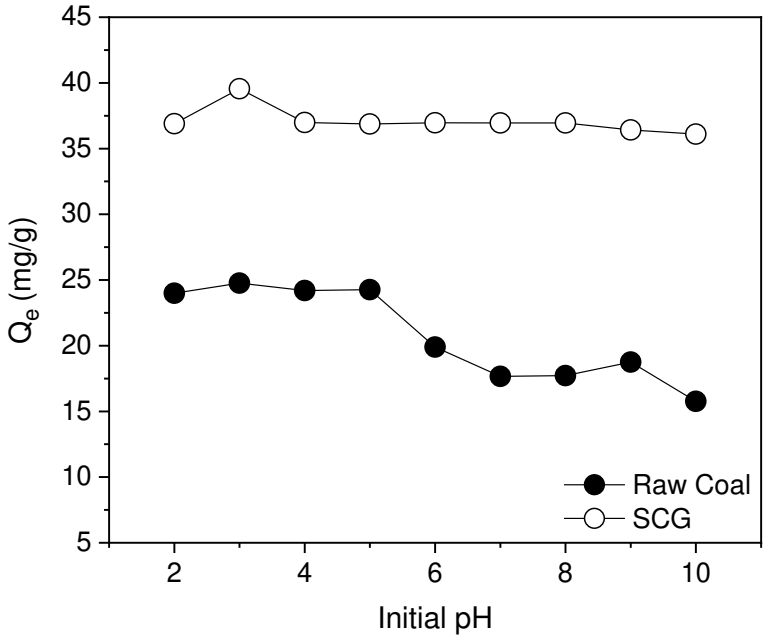

Figure 5. Effect of initial pH on the removal of Congo red dye by raw coal and SCG

Kinetic study

The effect of contact time on percentage removal of Congo red is shown in **Figures 6a** and **b**, for Raw Coal and SCG, respectively. In this study, the active sites of Raw Coal got saturated at 250 min and subsequently the adsorption of the dye onto the surface of the Raw Coal remained fairly constant till 360 min. In the case of SCG, the adsorption efficiency increased with time and reached the peak at 200 min. It is pertinent to say that the SCG reached equilibrium

time faster than the Raw Coal and the kinetic data showed that SCG performed better than Raw Coal in the removal of Congo red from aqueous solutions. The quick removal of the adsorbate at the beginning of the adsorption process as observed by Danish et al. (2011) is due to the number of vacant sites available on the surface of the adsorbent at the start of the adsorption process and relatively large number the adsorbate molecules present in the solution. The constant increase in adsorption and ultimately the attainment of equilibrium is due to the limited mass transfer of the dye molecules from the adsorbate solution to the surface of the adsorbent. To conduct equilibrium study, contact time of 300 min and 250 min were used for Raw Coal and SCG, respectively.

Adsorption kinetics plays a significant role in adsorption studies because it provides important information on various pathways and mechanisms of a reaction (Adebayo et al. 2020; Ribas et al. 2020). To elucidate the kinetics of adsorption in this study, pseudo-first order, pseudo-second order, Avrami fractional order and intraparticle diffusion models were used. The various parameters of these models could be used to determine the rate controlling mechanism of the entire adsorption process. The adjusted coefficient of determination (R^2_{adj}) and standard deviation (*SD*), as shown in respective **Equations 2** and **3**, were used to express the degree of correlation between the experimental values and the calculated data as well as to determine how kinetic data are well fitted. The *SD* values measure the differences between the observed or experimental values and the calculated or predicted values by the model. The smaller the *SD* value, the smaller the difference between the observed and calculated values, then the better the fit. The closer the R^2_{adj} value to unity, the better the fit of the model.

$$R^2_{adj} = \left\{1-(1-R^2)\right\}\left\{\frac{n-1}{n-p-1}\right\} \quad (2)$$

$$SD = \sqrt{\left\{\frac{1}{n-p}\right\}\sum_{i=1}^{n}\left(q_{i,\exp}-q_{i,model}\right)^2} \quad (3)$$

where q is the numerical value of the data, $q_{i,model}$ is an individual value predicted by the model; $q_{i,exp}$ is an individual q value obtained from the experiment, n represents the number of experiments performed; p is the number of fitting parameters in a specific model; and R^2 represents the determination coefficient.

The rate expressions from which the rate constants were obtained are presented in **Equations 4 – 7** for pseudo-first order, pseudo-second order, Avrami fractional order and intraparticle diffusion models, respectively.

$$Q_t = Q_e\left\{1-\exp(-k_f t)\right\} \quad (4)$$

$$Q_t = Q_e - \frac{Q_e}{k_s Q_e t + 1} \quad (5)$$

$$Q_t = Q_e\left\{1-\exp(-k_{Av}t)^{n_{Av}}\right\} \quad (6)$$

$$Q_t = k_{ipd}\sqrt{t} + C \quad (7)$$

where the quantity of dye removed at equilibrium is given as Q_e (mg/g) and the quantity adsorbed at a given time, *t,* is given as Q_t (mg/g), k_f (1/min) is the pseudo-first order rate constant, k_s (g/mg min) is the pseudo-second order rate constant, k_{Av} (1/min) represents the Avrami fractional order rate constant, n_{Av} is the Avrami fractional kinetic order that is related to the mechanism of adsorption, k_{ipd} (mg/g $min^{0.5}$) is the intraparticle mass transfer constant, and C (mg/g) represents the boundary layer.

Figures 6a and **b** present the kinetic curves of the Raw Coal and SCG, respectively, for removal of Congo red while **Table 2** presents the parameters of the models. From the table, *SD* values are 1.856 mg/g and 1.521 mg/g (pseudo-first order), 0.7212 mg/g and 1.143 mg/g (pseudo-second order), and 0.2199 mg/g and 0.3433 mg/g (Avrami model) for Raw Coal and SCG, respectively. It is evident that the kinetic profile of the adsorption process did not follow pseudo-first order and pseudo-second order kinetic model but followed the Avrami fractional order kinetic model. Avrami fractional-order kinetic model is an empirical model that has been used to explain the solid-solution interface characteristics of adsorption systems (Lima et al. 2016; Thue et al., 2016; Adesemuyi et al. 2020). The Avrami model perfectly describes the kinetics of adsorption of Congo red onto the two materials because the model presents the lowest values of the SD as well as the highest values of R^2_{adj}. The values of k_{Av} are 0.02066 1/min (Raw Coal) and 0.02684 1/min (SCG). These values signify that the rate of adsorption of Congo red onto SCG was slightly faster than that of Raw Coal. This observation also corroborates the observation stated earlier that SCG reached equilibrium (equilibrium time of 200 min) earlier than Raw Coal (equilibrium time of 250 min). The average fractional order of the adsorption process is 0.7585.

To investigate the mechanism of the adsorption process, the intraparticle diffusion model was used to interpret the kinetic data. The intraparticle plots, **Figure 6c** (Raw Coal) and **Figure 6d** (SCG), did not begin from the zero origin. Each plot has two linear regions, which indicate a two-step mechanism for the adsorption process (Adebayo et al. 2020). The first linear region shows the fast adsorption process in which Congo red molecules are transferred to the surface of the adsorbents (Adebayo et al. 2014; Adebayo et al. 2020). The second linear region represents the diffusion through small pores of the adsorbents. The second linear region is achieved after equilibrium was reached. It should, however, be noted that the adsorption process was not the controlling by diffusion. The intraparticle mass transfer rate constant for the first linear region ($k_{ipd,1}$) of SCG is higher than that of Raw Coal by a factor of *ca.* 2. This infers that the molecules of Congo red migrate to the surface of the SCG faster that to the surface of the Raw Coal.

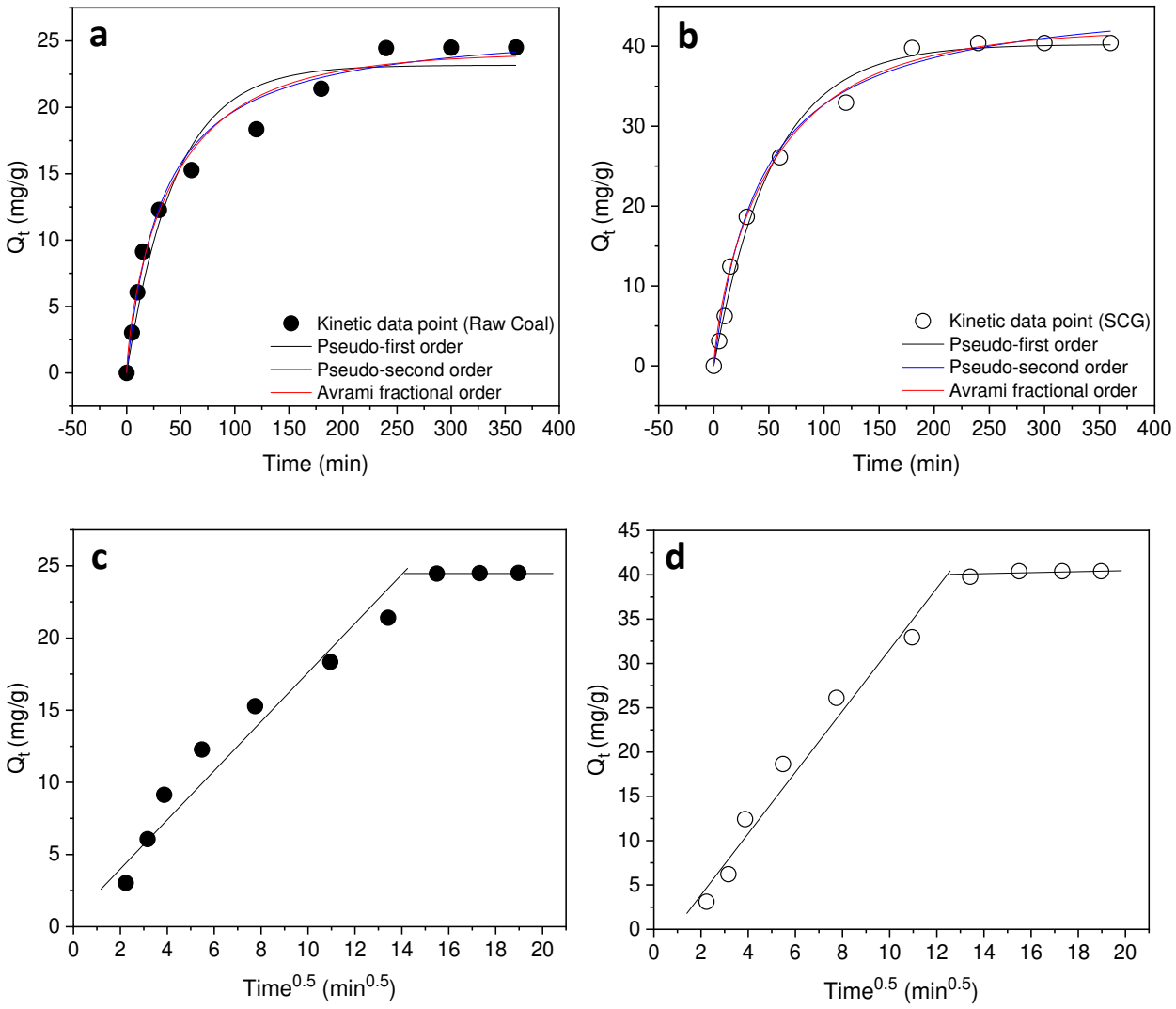

258

259

260 **Figure 6**. Kinetic plots (**a** and **b**) and intraparticle diffusion plots (**c** and **d**) of Raw Coal (**closed circles**) and SCG

261 (**open circles**)

262 **Table 2. Kinetic parameters of Congo red adsorption onto Raw Coal and SCG**

	Raw Coal	**SCG**
Pseudo-first order		
$Q_{e,cal}$ (mg/g)	24.46	40.41
$Q_{e,exp}$ (mg/g)	23.18	40.22
k_f (1/min)	0.02223	0.01859
SD (mg/g)	1.856	1.521
R^2_{adj}	0.9617	0.9921
Pseudo-second order		
$Q_{e,exp}$ (mg/g)	26.432	46.97
k_s (g/mg min)	0.001120	4.880×10^{-4}

SD (mg/g)	0.7212	1.143
R^2_{adj}	0.9801	0.9852
Avrami fractional order		
$Q_{e,exp}$ (mg/g)	24.13	42.15
k_{Av} (1/min)	0.02066	0.02684
n_{Av}	0.7457	0.7713
SD (mg/g)	0.2199	0.3433
R^2_{adj}	0.9986	0.9990
Intraparticle diffusion		
$k_{ipd,1}$	1.5287	3.467
C	1.985	–2.750
R^2_{adj}	0.9436	0.9520

263

264 **Adsorption isotherms**

265 The dependences of Congo red uptakes on the equilibrium concentrations are shown in **Figures 7a** and **7b** for Raw
266 Coal and SCG, respectively, at 25 °C. The concentration dependent study was done by varying concentrations of
267 Congo red from 25 mg/L to 800 mg/L at various temperature values of 25, 35, 45, 55 and 65 °C. To properly
268 understand the characteristics of the adsorption process, it is important to analyze equilibrium experimental data using
269 appropriate adsorption models. In this study, the Langmuir, Freundlich, Liu and Dubinin-Radushkevich isothermal
270 models were employed to analyze equilibrium experimental data for the adsorption of the Congo red dye onto the
271 adsorbents. The respective equations of Langmuir, Freundlich, Liu and Dubinin-Radushkevich models are provided
272 in **Equations 8** – **11**, respectively.

273 $$Q_e = \frac{Q_{\max} K_L C_e}{1 + K_L C_e} \quad (8)$$

274 $$Q_e = K_F C_e^{\frac{1}{n_F}} \quad (9)$$

275 $$Q_e = \frac{Q_{\max} (K_g C_e)^{n_g}}{1 + (K_g C_e)^{n_g}} \quad (10)$$

276 $$Q_e = Q_{\max} \exp\left\{ -K_{DR} RT \ln\left[1 + \frac{1}{C_e} \right]^2 \right\} \quad (11)$$

where C_e (mg/L) represents Congo red concentration at equilibrium (after adsorption process), Q_{max} (mg/g) represents the maximum adsorption capacity of the adsorbent, K_L = Langmuir equilibrium constant (L/mg), K_F (mg/g (mg/L)$^{-1/nF}$) is the Freundlich equilibrium constant, n_F = heterogeneity factor, K_g (L/mg) represents the Liu equilibrium constant, n_g is the dimensionless exponent of the Liu model, K_{DR} (mol^2/kJ^2) is the Dubinin-Radushkevich constant, which is related to the energy of adsorption, R (8.314 J/mol K) is the universal gas constant, and T (K) is the absolute temperature.

The modeling of the equilibrium data to the isothermal models are shown in **Figure 7** at 25 °C while the parameters of the models are presented in **Tables 3** and **4** for respective data of Raw Coal and SCG at 25 °C – 65 °C. The Liu model is the best model that described well the adsorption of Congo red onto Raw Coal and SCG at all experimental temperature values on the basis of the SD and R^2_{adj} values. It is therefore correct to discuss only the parameters of the Liu model.

The Liu model is a three-parameter isotherm model that assumes that the active binding sites of the adsorbent cannot possess the same energy (Liu et al. 2003). The adsorbent surface will therefore present active sites that the adsorbate molecules can preferentially occupy, hence, the preferred active sites will be saturated with the adsorbate molecules (Liu et al. 2003). Since the Liu model is the best model for description of the equilibrium adsorption data, then the active sites of the Raw Coal and SCG possessed different energy (Liu et al. 2003; Rovani et al. 2014). The values maximum adsorption capacities (Q_{max}) are 109.1 mg/g and 129.0 mg/g, respectively, which are obtained at 25 °C. The values of K_g increase steadily as the temperature increases. This phenomenon signifies that an increase in temperature favor the adsorption of Congo red onto Raw Coal and SCG, hence, the adsorption process is endothermic (Rovani et al. 2014). The n_g values vary between 0.5267 and 1.340 for Raw Coal and between 0.3021 and 0.9337 for SCG as temperature increases.

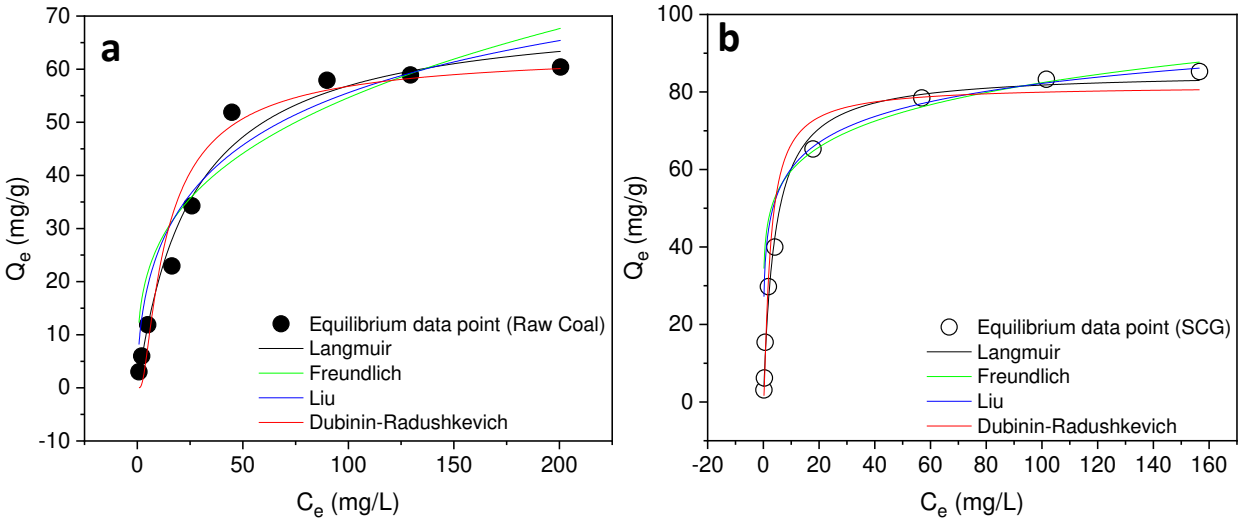

Figure 7. Isotherm plots Raw Coal (**a**) and SCG (**b**) at 25 °C

301 **Table 3.** Isotherm parameters of Raw Coal

Temperature (°C)	**25**	**35**	**45**	**55**	**65**
Langmuir					
Q_{max} (mg/g)	71.45	71.40	76.88	81.86	82.03
K_L (L/mg)	0.03903	0.04432	0.04441	0.04486	0.05972
SD (mg/g)	3.473	3.0448	3.156	4.279	5.311
R^2_{adj}	0.9787	0.9841	0.9852	0.9760	0.9658
Freundlich					
K_F (mg/g (mg/L)$^{-1/nF}$)	13.24	9.751	10.07	10.67	12.73
n_F	3.248	2.680	2.601	2.581	2.749
SD (mg/g)	3.275	7.903	7.953	8.569	10.24
R^2_{adj}	0.9400	0.8928	0.9062	0.9036	0.8730
Liu					
Q_{max} (mg/g)	109.1	66.19	72.14	75.45	75.70
K_g (L/mg)	0.02072	0.03181	0.05156	0.05764	0.06993
n_g	0.5267	1.262	1.187	1.275	1.340
SD (mg/g)	1.350	2.793	3.122	4.201	5.219
R^2_{adj}	0.9908	0.9866	0.9856	0.9859	0.9757
Dubinin-Radushkevich					
Q_{max} (mg/g)	63.65	66.63	71.35	76.58	78.19
K_{DR} (mol^2/kJ^2)	0.002250	0.002570	0.002500	0.002570	0.002090
SD (mg/g)	4.401	4.099	4.470	5.168	6.188
R^2_{adj}	0.9043	0.9711	0.9703	0.9650	0.9536

302

303 **Table 4.** Isotherm parameters of SCG

Temperature (°C)	**25**	**35**	**45**	**55**	**65**
Langmuir					
Q_{max} (mg/g)	85.17	93.77	98.12	106.23	117.6
K_L (L/mg)	0.2411	0.1357	0.1007	0.0917	0.06213
SD (mg/g)	2.939	2.072	2.279	4.758	4.080
R^2_{adj}	0.9923	0.9967	0.9962	0.9858	0.9907
Freundlich					
K_F (mg/g (mg/L)$^{-1/nF}$)	43.23	19.75	18.29	18.37	16.68
n_F	7.145	3.085	2.914	2.796	2.572

SD (mg/g)	4.936	8.986	9.120	10.23	10.44
R^2_{adj}	0.8092	0.9378	0.9385	0.9342	0.9394
Liu					
Q_{max} (mg/g)	129.0	98.81	102.8	113.4	121.7
K_g (L/mg)	0.05627	0.06431	0.07361	0.08649	0.1126
n_g	0.3021	0.8613	0.8881	0.8648	0.9337
SD (mg/g)	1.100	1.294	2.005	4.734	4.0125
R^2_{adj}	0.9951	0.9997	0.9980	0.9899	0.9997
Dubinin-Radushkevich					
Q_{max} (mg/g)	81.69	88.33	92.08	97.75	105.7
K_{DR} (mol^2/kJ^2)	4.230×10^{-4}	7.720×10^{-4}	0.001050	0.001010	0.001420
SD (mg/g)	5.010	5.816	5.853	7.522	7.390
R^2_{adj}	0.7944	0.9750	0.9747	0.9644	0.9696

304

305 The adsorption capacities of some studies on the adsorption of graphene materials for removal of Congo red were
306 compared with those of Raw Coal and SCG as shown in **Table 5**. The adsorption capacities of Raw Coal and SCG for
307 removal of Congo red were higher than of five graphene materials out of the nine listed in the table. This implies that
308 both Raw Coal and SCG can be effectively used for treatment of water contaminated with Congo red. In general, the
309 two low-cost adsorbent materials have a tendency to be used for the treatment of industrial effluent that contain toxic
310 dyes.

311 **Table 5.** Comparison of adsorption maximums of graphene for Congo red removal

Graphene Material	**Q_{max} (mg/g)**	**Model**	**Reference**
Raw Coal	109.1	Liu	*This study*
Synthesize Coal Graphene (SCG)	129.0	Liu	*This Study*
Magnetic Fe_3O_4@graphene nanocomposite	33.66	Langmuir	Yao et al. (2012)
Magnetic mesoporous titanium dioxide–graphene oxide	89.95	Langmuir	Li et al. (2014)
Graphene oxide/chitosan	294.12	Langmuir	Du et al. (2014)
Graphene oxide/poly(amidoamine)	198.0	Langmuir	Rafi et al. (2018)
Graphene–chitosan composite hydrogel	384.6	Langmuir	Omidi and Kakanejadifard (2018)
Magnesium oxide (MgO)-graphene oxide	237.0	Langmuir	Xu et al. (2018)

Exfoliated graphite	80.78	Langmuir	Pham et al. (2019)
In-based metal-organic frameworks	84.50	Langmuir	Wei et al. (2019)
Graphene oxide/magnesium oxide nanocomposite	26.49	Dubinin-Kaganer-Radushkevich	Fahdil et al. (2019)

312

313 **Thermodynamic study**

314 Effect of temperature on the adsorption of Congo red was studied using the experimental condition earlier stated under
315 isothermal study. An increase in the temperature of the system increases the value of the equilibrium constant (**Figure**
316 **8a**), however, the values of adsorption capacities do not follow a specific pattern, that is the values anomalously do
317 not depend on temperature.

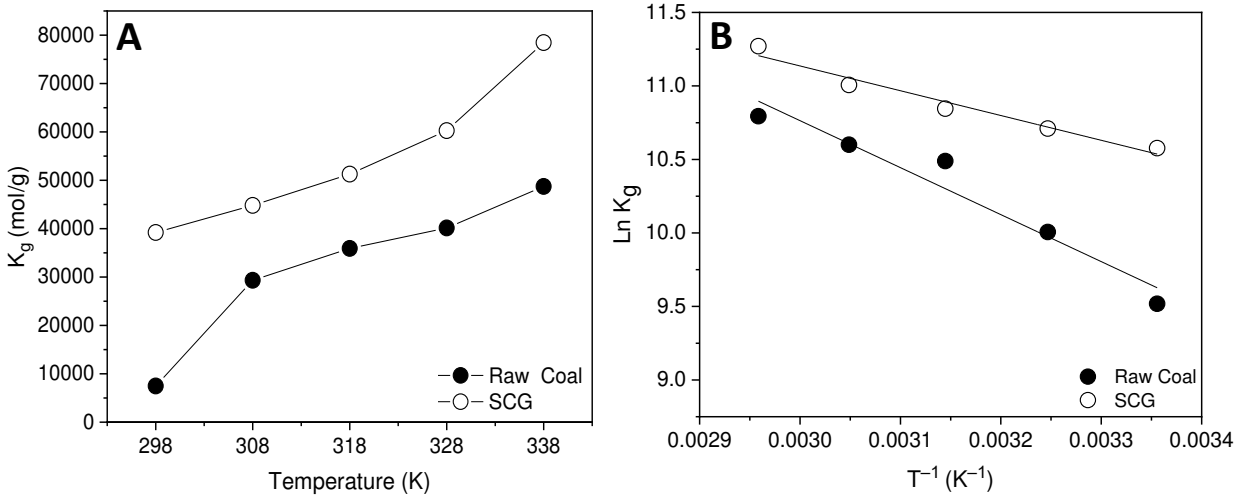

318

319 **Figure 8.** (**a**) Dependence of Liu constant (K_g) on temperature and (**b**) van't Hoff plot for the removal of Congo red
320 by Raw Coal and SCG

321 The thermodynamic parameter of standard Gibbs free energy ($\Delta G°$) is an important parameter that is determined to
322 predict the spontaneity of the adsorption system. The values of $\Delta G°$ as well as the values of standard enthalpy change
323 ($\Delta H°$) and standard entropy change ($\Delta S°$) were calculated using thermodynamic **Equations 12 – 14**. **Equation 14** is
324 generally known as van't Hoff thermodynamic equation.

325 $$\Delta G^o = \Delta H^o - T\Delta S^o \quad (12)$$

326 $$\Delta G^o = -RT\ln K \quad (13)$$

327 $$\ln K = -\frac{\Delta H^o}{R}\cdot\frac{1}{T} + \frac{\Delta S^o}{R} \quad (14)$$

where R is the universal gas constant, T is the absolute temperature (K), and K is the equilibrium constant obtained from the best fit model for the equilibrium data. In this case, Liu equilibrium constant, Kg, was used. The unit of the K_g was converted from L/mg to mol/g.

The $\Delta G°$ values ranged between –23.73 kJ/mol and –30.33 kJ/mol for Raw Coal and between –26.20 kJ/mol and –31.67 kJ/mol for SCG (**Table 6**). The negative values of $\Delta G°$ indicate that the adsorption was spontaneous and feasible at all temperatures for both adsorbents. The numerical values of $\Delta H°$ and $\Delta S°$ were obtained from the slope and intercept, respectively, of the van't Hoff plot (**Figure 8a**). The values of $\Delta H°$ are positive, which is an indication that the adsorption process was endothermic, this only reflects in the values of equilibrium constant (**Figure 8a**). The estimated values of $\Delta S°$, which are positive for adsorption of Congo red by Raw Coal and SCG, showed that the randomness at the solid-liquid interface increased (Adebayo 2019).

Table 6. Summary table of the thermodynamic parameters for Raw Coal and SCG

	Temperature (K)	**298**	**308**	**318**	**328**	**338**
Raw Coal	**$\Delta G°$ (kJ/mol)**	–23.73	–25.62	–27.73	–28.91	–30.33
	$\Delta H°$ (kJ/mol)	26.57				
	$\Delta S°$ (J/mol K)	169.2				
	R^2_{adj}	0.9269				
SCG	**$\Delta G°$ (kJ/mol)**	–26.20	–27.42	–28.67	–30.01	–31.67
	$\Delta H°$ (kJ/mol)	14.02				
	$\Delta S°$ (J/mol K)	134.6				
	R^2_{adj}	0.9526				

Conclusion

Coal based graphene was prepared from Nigeria's bituminous coal using chemical methods. The characterization of the adsorbent with XRD, SEM and SEM-EDX confirmed the formations of graphene material with distribution of large inter-agglomerate pores consisting carbon, which is the major constituent of graphene. Adsorption of Congo red on the synthesized adsorbent was investigated. The pH had no significant effect on SCG but significantly affect Raw Coal adsorption. Variations in contact time, initial Congo red concentrations and temperature significantly affected the adsorption of Congo red onto Raw Coal and SCG. Adsorption kinetics was studied using pseudo first order, pseudo-second order, Avrami and intraparticle diffusion models with Avrami fractional model as the most suitable model for description of the kinetic data of the adsorption process. The isotherm parameters were analyzed using Langmuir, Freundlich, Lu and Dubinin-Radushkevich models. It was observed that the adsorption is favorably fitted well to the Liu isotherm model. The maximum adsorption capacities of the raw coal and synthesized coal graphene obtained from the Liu model at 25 °C are 109.1 mg/g and 129.0 mg/g, respectively. The thermodynamic study showed an endothermic and a spontaneous adsorption process for both adsorbent materials. Synthesized coal graphene

perfumed better than the Raw Coal in the removal of Congo red from aqueous solutions. The Raw coal and SCG exhibited promising adsorption potentials for Congo red and thus can be used as low-cost and efficient adsorbents for wastewater treatment.

Ethical Approval

Not applicable

Consent to Participate

Not applicable

Consent to Publish

Not applicable

Authors Contributions

Temilolu J. Popoola: investigation, data acquisition, conceptualization, and preparation of the draft manuscript.

Afamefuna E. Okoronkwo: conceptualization, methodology, and supervision.

Olugbenga O. Oluwasina: methodology, editing and supervision.

Matthew A. Adebayo: data analysis, supervision, editing and review of the manuscript.

Funding

There was no funding for the research work.

Competing Interests

The authors declare that there is no competing interests.

Availability of data and materials

The data used in this study are available from the corresponding author on request.

References

Adebayo MA, Adebomi JI, Abe TO, Areo FI. (2020) Removal of Aqueous Congo Red and Malachite Green using Ackee Apple Seed–Bentonite Composite. Colloids Interface Sci Commun 38:100311. Doi: 10.1016/j.colcom.2020.100311

Adebayo MA (2019) Adsorption of congo red from aqueous solutions using clay–corn cob–$FeCl_3$ composite. FUTA J Res Sci 15:61–74

Adebayo MA, Prola LDT, Lima EC, Puchana-Rosero MJ, Cataluña R, Saucier C, Umpierres CS, Vaghetti JCP, da Silva LG, Ruggiero R. (2014) Adsorption of Procion blue MX-R dye from aqueous solutions by lignin chemically modified with aluminium and manganese. J Hazard Mater 268:43–50. Doi: 10.1016/j.jhazmat.2014.01.005

Adesemuyi MF, Adebayo MA, Akinola AO, Olasehinde FE, Adewole KA, Lajide L. (2020) Preparation and characterisation of biochars from elephant grass and their utilisation for aqueous nitrate removal: Effect of pyrolysis temperature J Environ Chem Eng 8:104507. Doi: 10.1016/j.jece.2020.104507

Alhashimi HA, Aktas CB. (2017) Life cycle environmental and economic performance of biochar compared with activated carbon: a meta-analysis. Resour Conserv Recycl 118:13–26

Ali I. (2012) New generation adsorbents for water treatment Chem Rev 112:5073–5091

Chong KY, Chia CH, Zakaria S, Sajab MS. (2014) Vaterite calcium carbonate for the adsorption of Congo red from aqueous solutions. J Environ Chem Eng 2:2156–2161

Cui L, Wang Y, Gao L, Hu L, Yan L, Wei Q, Du B. (2015) EDTA functionalized magnetic graphene oxide for removal of Pb(II), Hg(II) and Cu(II) in water treatment: Adsorption mechanism and separation property. Chem Eng J 281:1–10. Doi: 10.1016/j.cej.2015.06.043

Danish M, Hashim R, Rafatullah M, Sulaiman O, Ahmad A, Govind G. (2011) Adsorption of Pb(II) ions from aqueous solutions by date bead carbon activated with $ZnCl_2$. Clean-Soil, Air, Water 39:392–399

dos Santos DC, Adebayo MA, Pereira SFP, Prola LDT, Cataluña R, Lima EC, Gally CR, Saucier C, Machado FM. (2014) Application of carbon composite adsorbents prepared from coffee wastes and red mud for the removal of textile dyes from aqueous solutions: Kinetic, equilibrium, and thermodynamic studies. Korean J Chem Eng 31:1470–1479. Doi: 10.1007/s11814-014-0086-3

Du Q, Sun J, Li Y, Yang X, Wang X, Wang Z, Xia L. (2014) Highly enhanced adsorption of congo red onto graphene oxide/chitosan fibers by wet-chemical etching off silica nanoparticles. Chem Eng J 245:99–106. Doi: 10.1016/j.cej.2014.02.006

Fahdil A, Al-Niaimi D, Muhi FH. (2019) Kinetic and thermodynamic study on the removal of Congo red from the aqueous solution using graphene oxide/magnesium oxide nanocomposite. J Biochem Tech 4:1–10

Galashev AE, Polukhin VA. (2014) Removal of copper from graphene by bombardment with argon clusters: Computer experiment. Phys Met Metallogr 115:697–704

Ghann WE, Kang H, Uddin J, Chowdhury FA, Khondaker SI, Moniruzzaman M, Kabir MH, Rahman MM. (2019) Synthesis and characterization of reduced graphene oxide and their application in dye-sensitized solar cells. ChemEng 3:7. Doi: 10.3390/chemengineering3010007

Hairom NHH, Mohammad AW, Kadhum AAH. (2014) Nanofiltration of hazardous Congo red dye: performance and flux decline analysis. J Water Process Eng 4:99–106

Kumari S, Mankotia D, Chauhan G. (2016) Crosslinked cellulose dialdehyde for Congo red removal from its aqueous solutions. J Environ Chem Eng 4:1126–1136

Li L, Li X, Duan H, Wang X, Luo C. (2014) Removal of Congo red by magnetic mesoporous titanium dioxide–graphene oxide core–shell microspheres for water purification. Dalton Trans 43:8431–8438. Doi: 10.1039/c3dt53474j

Lima EC, Cestari AR, Adebayo MA. (2016) Comments on the paper: A critical review of the applicability of Avrami fractional kinetic equation in adsorption-based water treatment studies. Desalination Water Treat 57:19566–19571. Doi: 10.1080/19443994.2015

Liu Y, Xu H, Yang SF, Tay JH. (2003) A general model for biosorption of Cd^{2+}, Cu^{2+} and Zn^{2+} by aerobic granules. J Biotechnol 102:233–239

Nupearachchi CN, Mahatantila K, Vithanage M. (2017) Application of graphene for decontamination of water; implications for sorptive removal. Groundw Sustain Dev 5:206–215. Doi: 10.1016/j.gsd.2017.06.006

Omidi S, Kakanejadifard A. (2018) Eco-friendly synthesis of graphene–chitosan composite hydrogel as efficient adsorbent for Congo red. RSC Adv 8:12179. Doi: 10.1039/c8ra00510a

Pang LSK., Vassallo AM, Wilson MA. (1991) Fullerenes from coal. Nature 352:480

Pang LSK, Wilson MA. (1993) Nanotubes from coal. Energy Fuels 7:436–437

Pham VT, Tran TV, Nguyen TD, Tham NTH, Quang PTT, Uyen DTT, Le NTH, Vo DN, Thanh NT, Bach LG. (2019) Adsorption behavior of Congo red dye from aqueous solutions onto exfoliated graphite as an adsorbent: Kinetic and isotherm studies. Mater Today: Proceedings 18:4449–4457

Querol X, Fernández-Turiel JL, Lopez-Soler A. (1995) Trace elements in coal and their behaviour during combustion in a large power station. Fuel 74:331–343

Rafi M, Samiey B, Cheng C. (2018) Study of adsorption mechanism of Congo red on graphene oxide/PAMAM nanocomposite. Mater 11:496. Doi: 10.3390/ma11040496

Rao A., Raj AM, Manoj B. (2017) Extraction and characterization of preformed mixed phase graphene sheets from graphitized sub-bituminous coal. Asian J Chem 29:2425–2428. Doi: 10.14233/ajchem.2017.20722

Rehman A, Zulfiqar S, Shakir I, Aly Aboud MF, Shahid M, Warsi MF. (2020) Nanocrystalline hematite a-Fe_2O_3 synthesis with different precursors and their composites with graphene oxide. Ceram Int 46:8227–8237. Doi: 10.1016/j.ceramint.2019.12.050

Repo E, Koivula R, Harjula R, Sillanpää M. (2013) Effect of EDTA and some other interfering species on the adsorption of Co(II) by EDTA-modified chitosan. Desalination 321:93–102

Ribas MC, Franco M, Adebayo MA, Parkes GM, Lima EC, Féris LA. (2020) Adsorption of Procion Red MX-5B dye from aqueous solution using a homemade peach activated carbon compared with commercial activated carbon. Appl Water Sci 10:154. Doi: 10.1007/s13201-020-01237-9

Robinson T, McMullan G, Marchant R, Nigam P. (2001) Remediation of dyes in textile effluent: a critical review on current treatment technologies with a proposed alternative. Bioresour Technol 77:247–25

Rovani S, Fernandes A., Prola LDT, Lima EC, Santos WO, Adebayo MA. (2014) Removal of Cibacron Brilliant Yellow 3G-P Dye from aqueous solutions by Brazilian peats as biosorbents. Chem Eng Commun 201:1431–1458. Doi: 10.1080/00986445.2013.81695

Shin SR, Li Y, Jang HL, Khoshakhlagh P, Akbari M, Nasajpour A, Zhang YS, Tamayol A, Khademhosseini A. (2016) Graphene-based materials for tissue engineering. Adv Drug Deliv Rev 105:255–274

Shinn JH. (1996) Visualization of complex hydrocarbon reaction systems. Prepr of Pap – Am Chem Soc Div Fuel Chem 41:510–515

Sohn HI, Gordin ML, Xu T, Chen S, Lv D, Song J, Manivannan A, Wang D. (2014) Porous spherical carbon / sulphur nanocomposite by aerosol synthesis: The effect of pore structure and morphology on their electrochemical performance as Lithium/sulphur battery cathodes. ACS Appl Mater Interfaces 6:596–606

Stephen LU. (2000) Ultraviolet/Visible Light Adsorption Spectrometry in clinical Chemistry., John Wiley and Sons Ltd, Chichester, pp 1699–171

Suhas PJM, Carrott MML, Carrott R, Singh R, Singh LP, Chaudhary M. (2017) An innovative approach to develop microporous activated carbons in oxidising atmosphere. J Clean Prod 156:549–555

Suraj G, Iyer C, Rugmini S, Lalithambika M. (1997) The effect of micronization on kaolinites and their sorption behavior. Appl Clay Sci 12:111–130.

Tabrez AK, Kumar D. (2004) Removal of some basic dyes from artificial wastewater by adsorption on Akash Kinari Coal. J Sci Ind Res 63:355–364

471 Thue PS, Adebayo MA, Lima EC, Sieliechi JM, Machado FM, Dotto GL, Vaghetti JCP, Dias SLP. (2016) Preparation,
472 characterization and application of microwave-assisted activated carbons from wood chips for removal of phenol from
473 aqueous solution. J Mol Liq 223:1067–1080. Doi: 10.1016/j.molliq.2016.09.032

474 Vassilev SV. (1994) Trace elements in solid waste products from coal burning at some Bulgarian thermoelectric power
475 stations. Fuel 73:367–374

476 Ward CR, Spears DA, Booth CA, Staton I. (1999) Mineral matter and trace elements in coals of the Gunnedah Basin
477 New South Wales. Australia Int J Coal Geol 40:281–308

478 Weber J, Wolfe N. (1987) Kinetic studies of the reduction of aromatic azo dyes in anaerobic waste water. Environ
479 Toxicol Chem 6:911–919

480 Wei F, Ren Q, Liang Z, Chen D. (2019) Synthesis of graphene oxide/metal-organic frameworks composite materials
481 for removal of Congo red from wastewater. ChemistrySelect 4:5755–5762. Doi: 10.1002/slct.201900363

482 Xu J, Xu D, Zhu B, Cheng B, Jiang C. (2018) Adsorptive removal of an anionic dye Congo red by flower-like
483 hierarchical magnesium oxide (MgO)-graphene oxide composite microspheres. Appl Surf Sci 435:1136–1142. Doi:
484 10.1016/j.apsusc.2017.11.232

485 Yang Q, Choi H, Dionysiou DD. (2008) Nanocrystalline cobalt oxide immobilized on titanium dioxide nanoparticles
486 for the heterogeneous activation of peroxymonosulfate. Appl Catal B Environ 74:170–178

487 Yao J, Wen D, Shen J, Wang J. (2016) Zero discharge process for dyeing wastewater treatment. J Water Process Eng.,
488 11:98–103

489 Yao Y, Miao S, Liub S, Ma LP, Sun H, Wang S. (2012) Synthesis, characterization, and adsorption properties of
490 magnetic Fe_3O_4@graphene nanocomposite. Chem Eng J 184:326–332. Doi: 10.1016/j.cej.2011.12.017

491 Zhang Y, Yan L, Xu W, Guo X, Cui L, Gao L, Wei Q, Du B. (2014) Adsorption of Pb(II) and Hg(II) from aqueous
492 solution using magnetic $CoFe_2O_4$-reduced graphene oxide. J Mol Liq 191:177–182

Figures

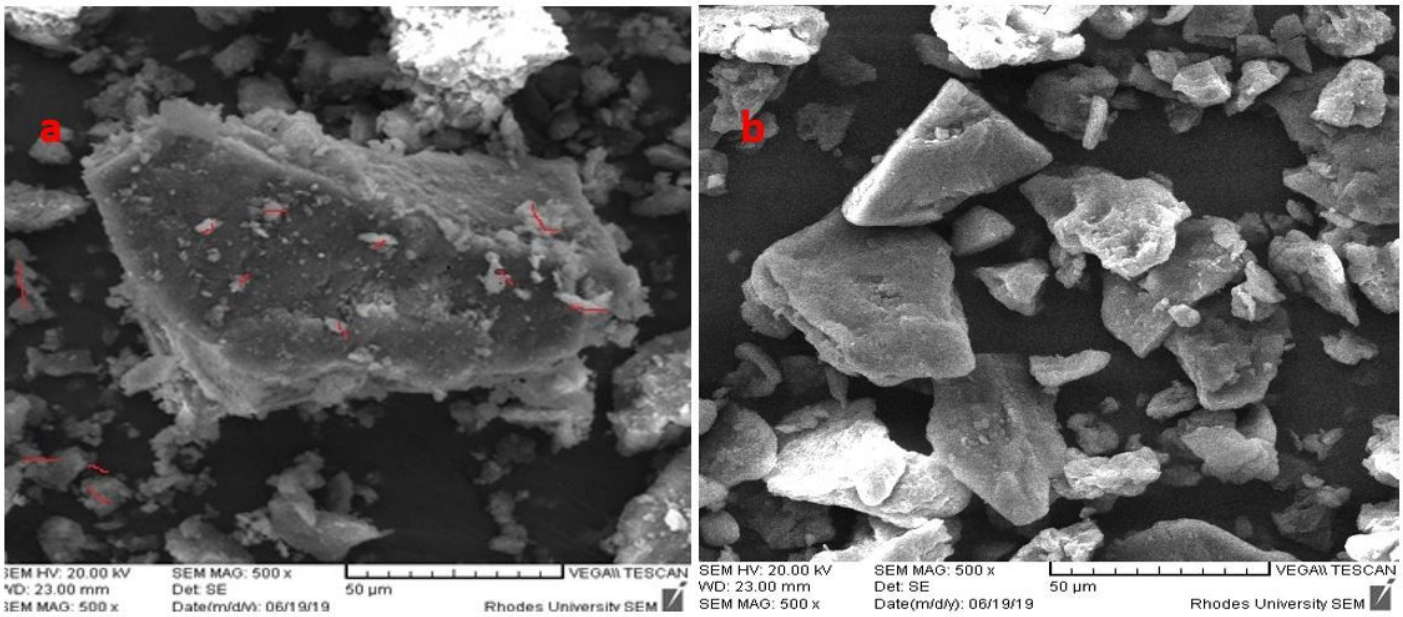

Figure 1

Scanning electron micrographs at 500x magnification of (a) Raw Coal and (b) SCG

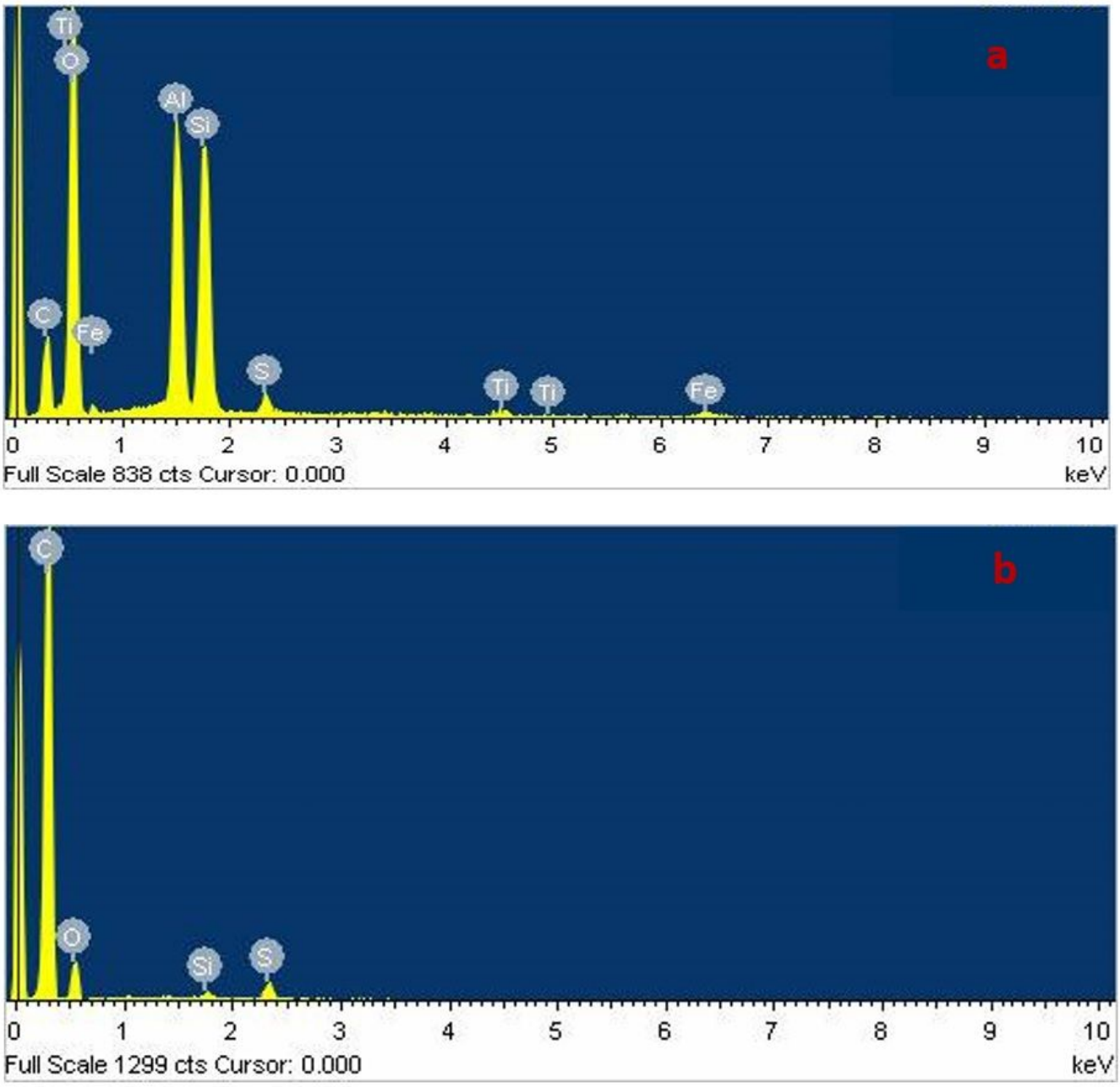

Figure 2

Energy-dispersive X-ray spectra of (a) Raw Coal and (b) SCG

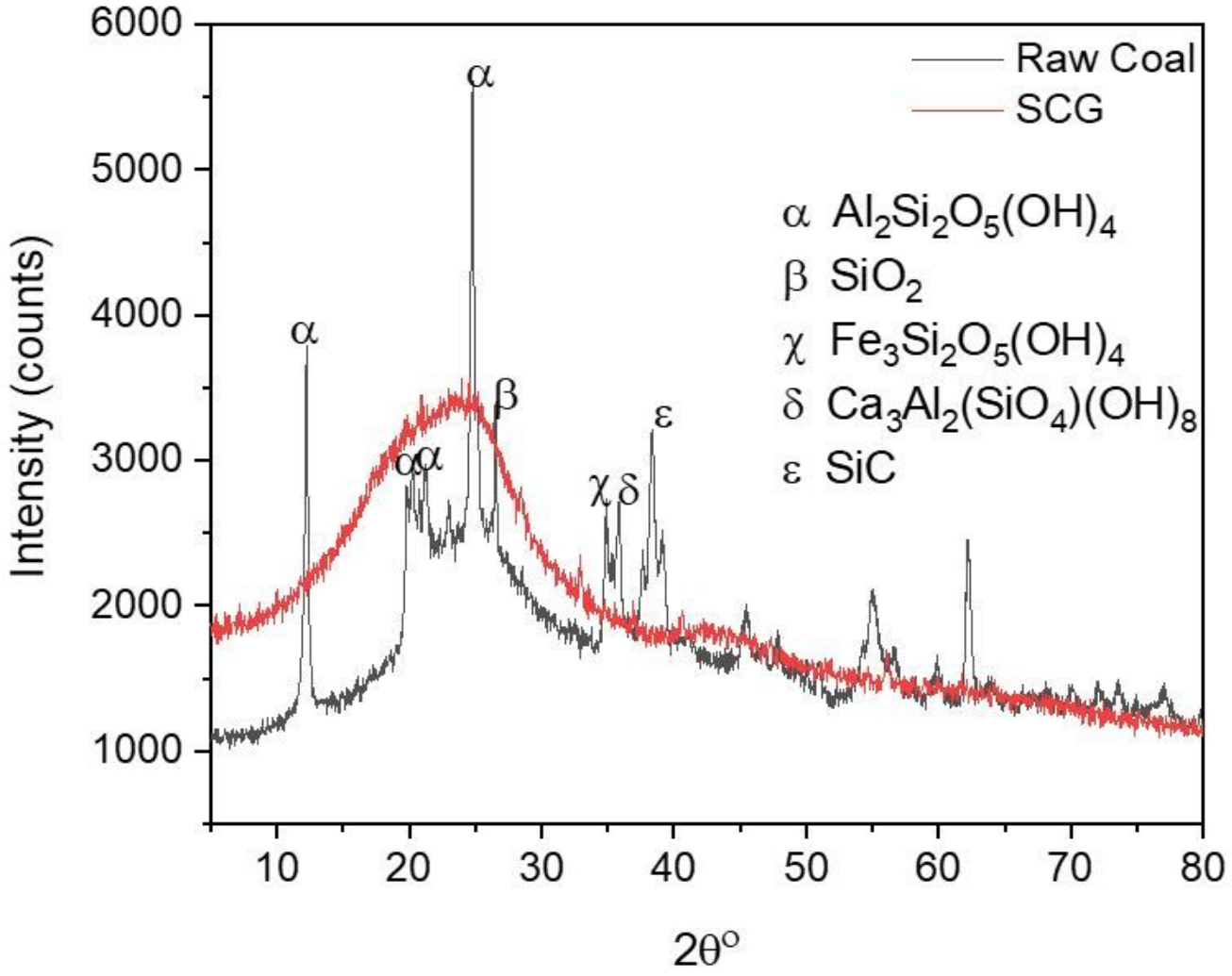

Figure 3

X-ray diffraction patterns of Raw Coal and SCG

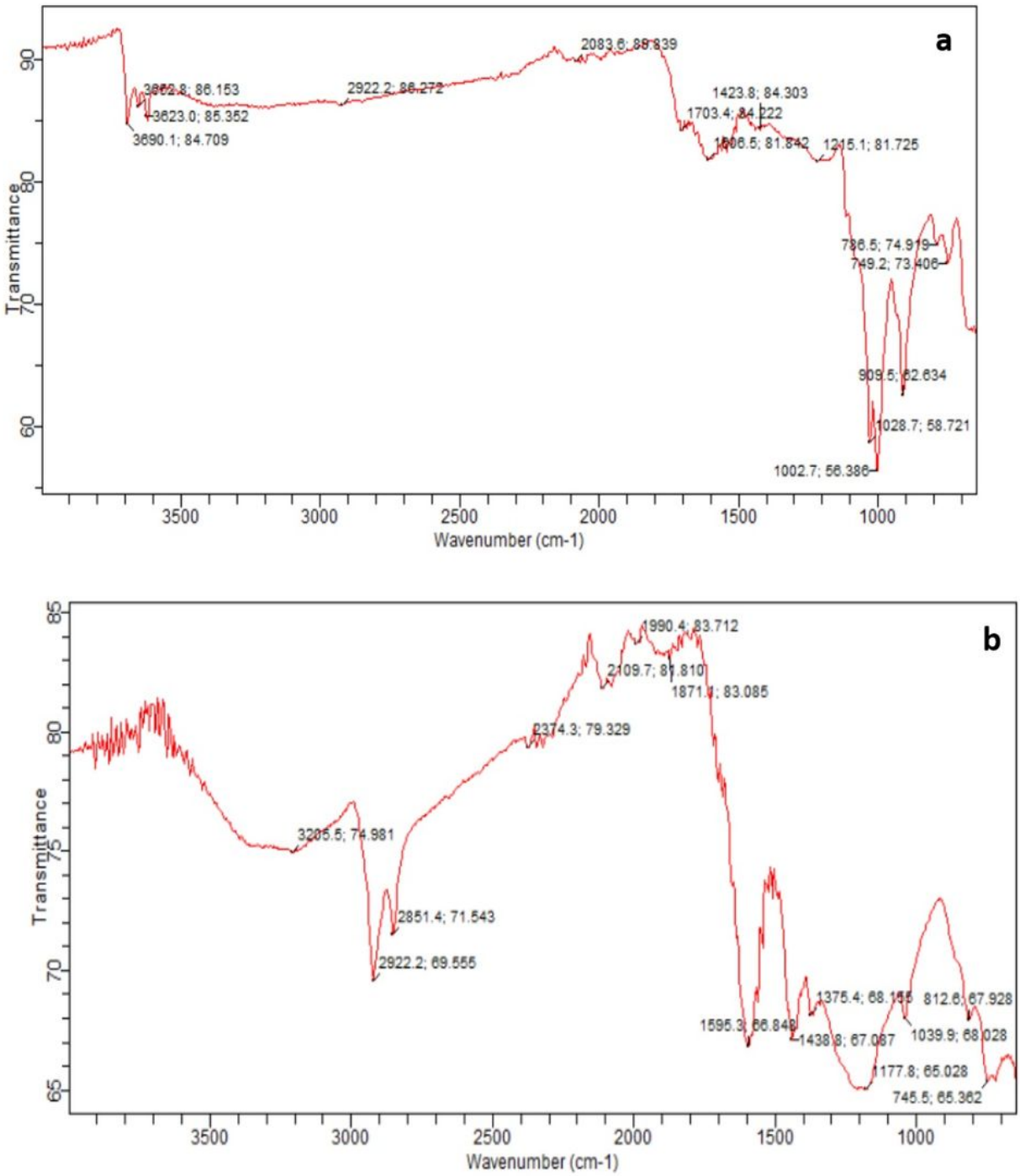

Figure 4

Fourier transform infrared spectra of (a) SCG before adsorption of Congo red and (b) SCG after adsorption of Congo red

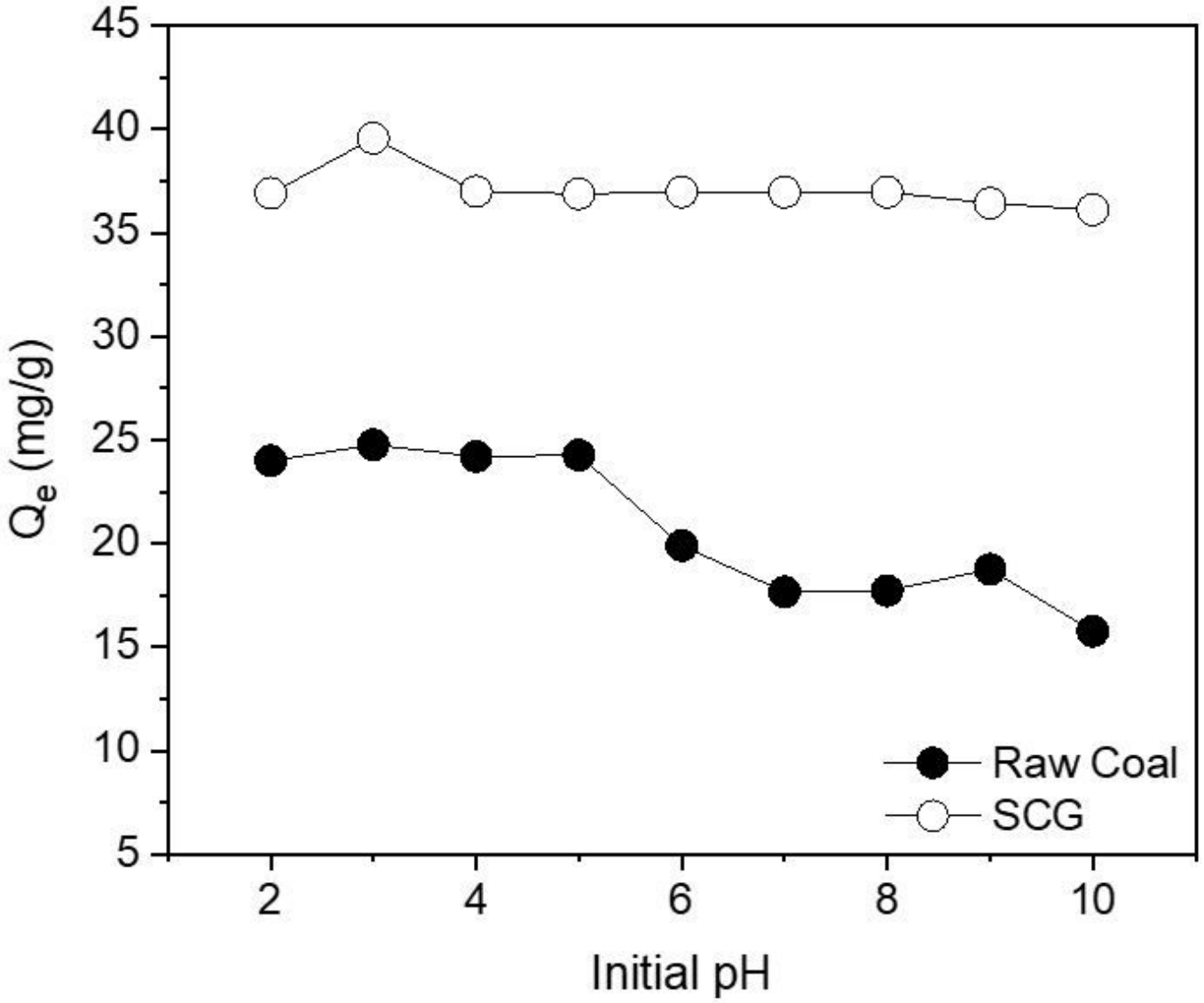

Figure 5

Effect of initial pH on the removal of Congo red dye by raw coal and SCG

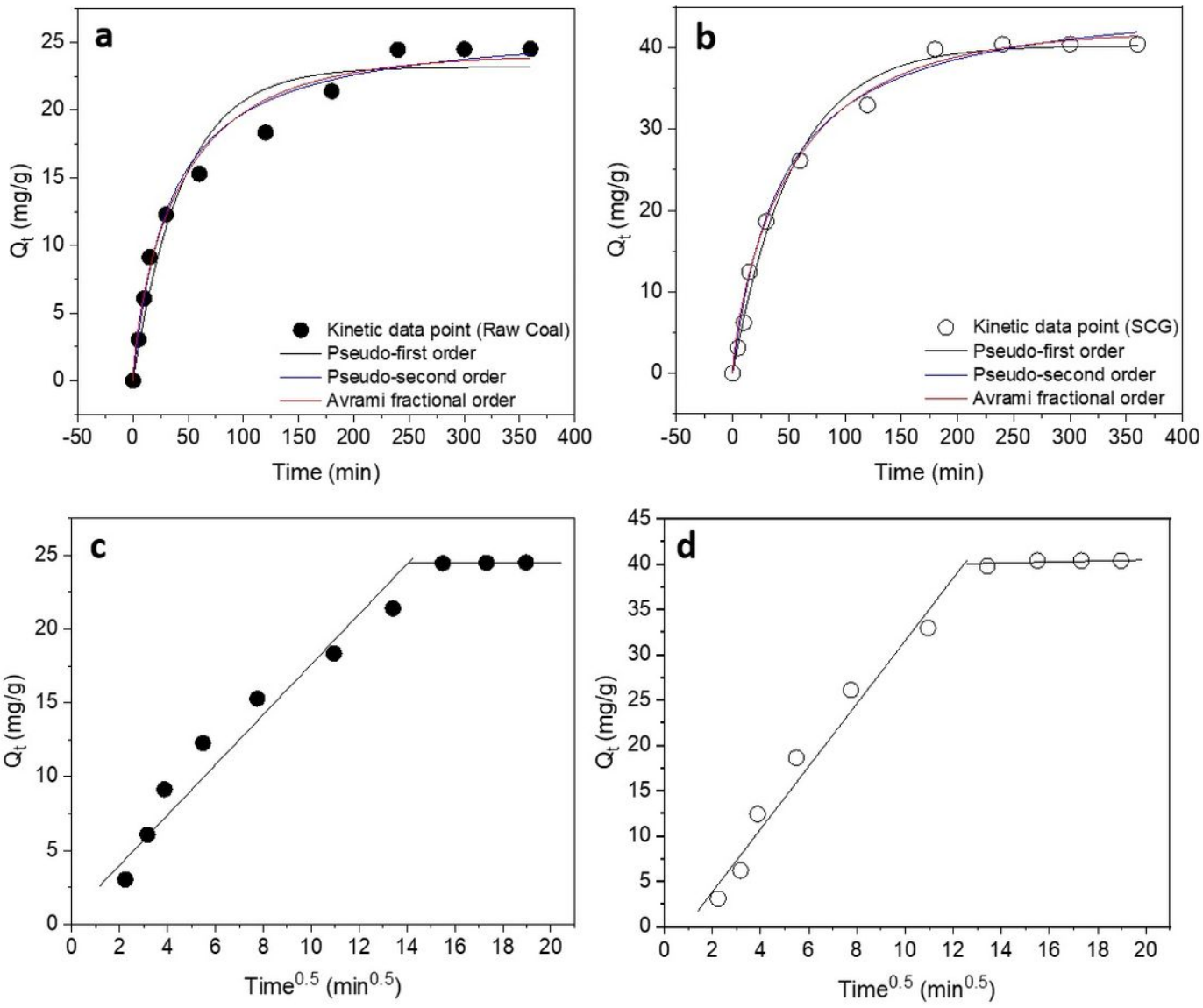

Figure 6

Kinetic plots (a and b) and intraparticle diffusion plots (c and d) of Raw Coal (closed circles) and SCG (open circles)

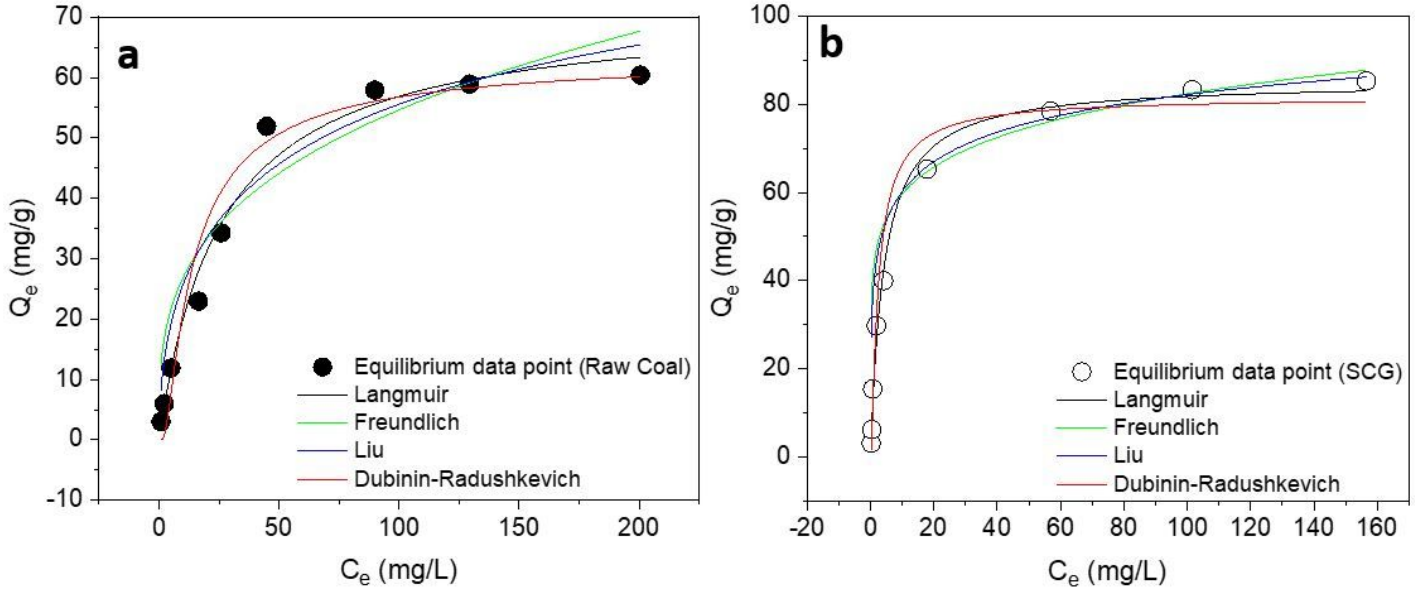

Figure 7

Isotherm plots Raw Coal (a) and SCG (b) at 25 °C

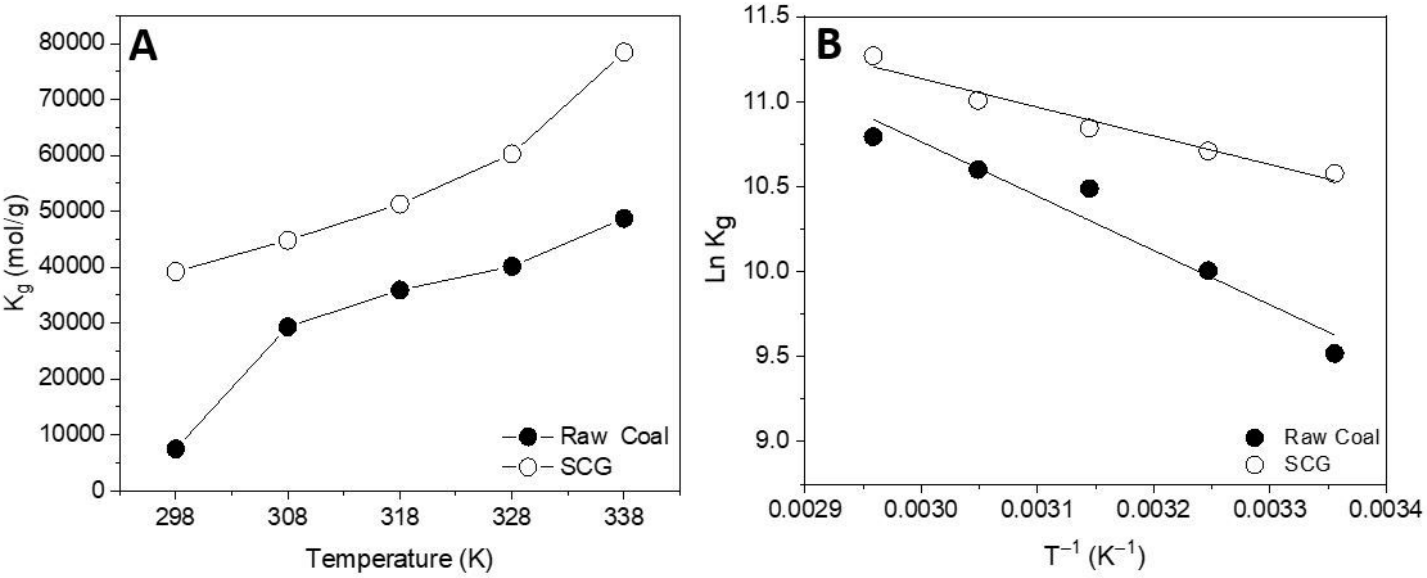

Figure 8

(a) Dependence of Liu constant (Kg) on temperature and (b) van't Hoff plot for the removal of Congo red by Raw Coal and SCG